Miniaturized magnet-less RF electron trap. I. Modeling and analysis

Aram H. Markosyan[a)]
Electrical Engineering and Computer Science Department, University of Michigan, Ann Arbor, Michigan 48109

Scott R. Green,[b)] Shiyang Deng,[c)] and Yogesh B. Gianchandani[d)]
Center for Wireless Integrated MicroSensing and Systems (WIMS²), University of Michigan, Ann Arbor, Michigan 48109

Mark J. Kushner[e)]
Electrical Engineering and Computer Science Department, University of Michigan, Ann Arbor, Michigan 48109

Ionization of trace gases by electron impact followed by ion extraction is an important pumping approach in ultrahigh vacuum (UHV) systems, which operate at nTorr pressure levels. However, pumping efficiency can only be achieved if the lifetime of electrons is sufficiently long to allow ionizing collisions with neutral species. In miniaturized systems, the electron lifetime is limited due to wall collisions. A traditional approach for an extended electron lifetime via trapping uses crossed electric and magnetic fields. These magnetic fields are undesirable in certain miniaturized systems such as atomic clocks. In this paper, the authors report a method and miniaturized structure for electron trapping in UHV conditions, which does not rely on magnetic fields. Electrons from an electron-beam source are transferred through a grid electrode into a central region of the device where they are trapped in lengthened trajectories using applied radio frequency (RF) electric fields. This paper describes analytical and numerical modeling to identify critical operating constraints between the trap geometry and driving RF voltage and frequency. An analytical relation is derived between RF voltage and frequency that should result in electron trapping for a given trap geometry. A plasma transport model is used to numerically investigate the trapping efficiency of the method with a two-dimensional geometry representative of experimental prototypes. A parametric study of RF voltage and frequency, electron beam current and initial energy, and background gas pressure demonstrates the efficacy of this approach in a miniaturized trap ($\approx 1\,cm^3$ trap volume). The authors find an increase of 3–4 orders of magnitude in electron density in the trap ($2 \times 10^7\,cm^{-3}$) compared to the density of the electron beam ($1 \times 10^3\,cm^{-3}$) with a proper choice of the applied voltage amplitude and RF frequency (typically 150 V and 150 MHz). These results indicate that miniature magnet-less electron traps can be effective. © 2017 American Vacuum Society.
[http://dx.doi.org/10.1116/1.4984751]

I. INTRODUCTION

On-board vacuum generation and maintenance are essential in microsystems that require very precise control over package pressure over long periods of deployment.[1] For example, some miniaturized atomic clocks and inertial sensors require low operating pressure to minimize spurious collisions between atomic vapor species and contaminating gas molecules.[2–10] However, the pressure of even a hermetically sealed package can significantly increase over time due to leakage into the cavity from the ambient and by outgassing from interior surfaces of the vacuum cavity. Conventional passive methods to mitigate this problem include the use of getters and low leakage packaging techniques.[11–16] However, in applications that require ultrahigh vacuum (UHV, nTorr levels), these methods typically cannot meet requirements over a reasonable length of deployment. In particular, gettering of atomic helium is a challenge, as helium easily permeates into the package from the ambient, and is not adsorbed onto typical getters.[17,18]

In contrast to conventional passive vacuum maintenance methods, a miniaturized active pump can potentially provide a stable vacuum environment at the chip scale. However, ultrahigh vacuum levels are not practically realized by chip-scale mechanical roughing pumps,[19,20] as the compressibility of the gas is too high for such pumps to operate efficiently in this pressure regime. Such vacuum levels are also not easily met by chip-scale thermal transpiration (Knudsen) pumps,[21] as the required dimensional scaling of molecular flow channels at low pressures works against the technique. However, a miniaturized ion pump holds significant promise for meeting UHV requirements.

Miniaturized ion pumps typically utilize a Penning cell structure similar to that used in commercial macroscale ion pumps.[16,22,23] The Penning cell structure consists of three electrodes (an anode and two cathodes) and magnets. The titanium cathodes are planar and are placed perpendicular to the long axis of the cylindrical-shaped anode, as shown in Fig.

a)Present address: Sandia National Laboratory, Livermore, CA 94550; electronic mail: amarkos@sandia.gov
b)Electronic mail: greensr@umich.edu
c)Electronic mail: kevindsy@umich.edu
d)Electronic mail: yogesh@umich.edu
e)Electronic mail: mjkush@umich.edu

1(a). The magnetic field is perpendicular to the cathode plates and oriented along the axis of the anode cylinder. Applying a large electrical field between the anode and the cathodes generates high energy electrons following electron emission from the cathodes. These electrons are confined to move in long spiral trajectories inside the cylindrical anode under crossed electrical and magnetic fields. The helical motion of the electrons produces a long path as the electron traverses from the cathode to the anode, which increases the probability of an electron colliding with gas molecules, which are then ionized. Ions are accelerated toward the titanium cathodes with sufficient energy to sputter titanium atoms. The reactive background gas molecules (oxygen and nitrogen, for example) are chemically adsorbed by the gettering action of exposed titanium on the cathode, while inert gas molecules (such as helium and argon) are ionized and implanted into the cathodes. Miniaturized chip-scale Penning cells for sputter-ion pumping have been reported to operate at pressures as low as $1.5\,\mu$Torr in a $2.5\,\text{cm}^3$ package.[24] This previously reported pump reduced pressure to <10 mTorr from a starting pressure of 115 mTorr in ≈ 4 h of operation with 450–600 V applied across the device and with a 100–250 mW power
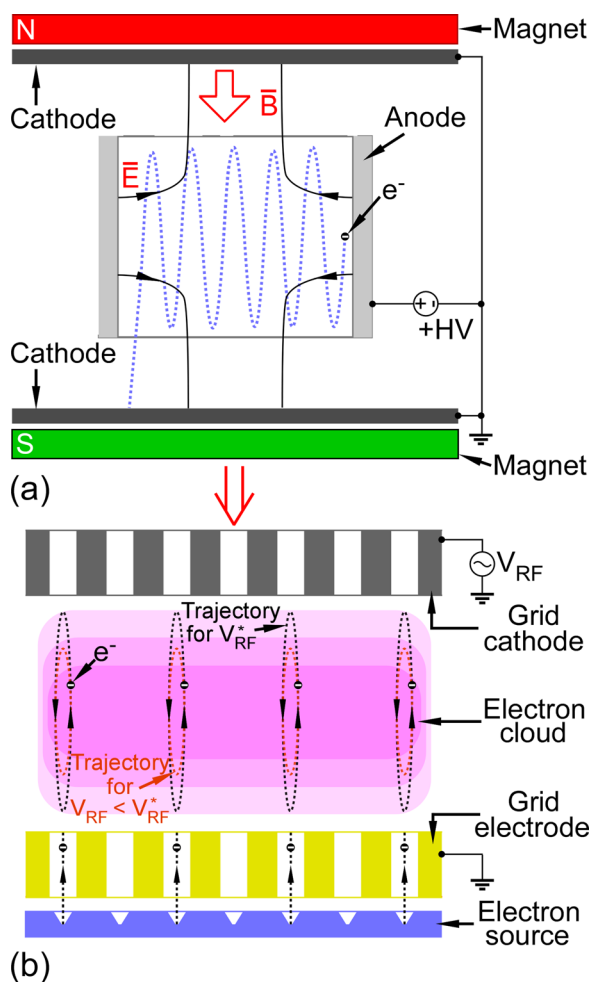

(a)

(b)

FIG. 1. (Color online) Schematics of electron trapping geometries: (a) the Penning cell electron trap, which requires crossed electrical and magnetic fields to trap electrons. (b) The RF electron trap, which does not require magnets to trap electrons.

consumption. A similar approach demonstrated pumping at pressures as low as $4\,\mu$Torr.[25]

In order to effectively employ miniaturized ion pumps for active pumping of atomic microsystems, such as chip-scale atomic clocks, several challenges still need to be addressed. The sub-μTorr pressures require long-lived electrons for efficient ionization, as the mean free path for ionizing collisions at these pressures far exceeds the dimensions of the cell. These long-lived electrons can be achieved with structures such as a Penning cell array. However, atomic systems which rely on specific spacing of energy levels are sensitive to magnetic fields, as these alter the quantum states of the atoms.[26,27] As a result, in atomic inertial microsystems, the final atomic state that is measured is altered by conditions unrelated to the size of the inertial field. This sensitivity to magnetic fields makes the Penning cell configuration less desirable for atomic microsystems because of the typically large magnitude of the magnetic fields required for electron trapping and the challenges associated with shielding such fields and minimizing field gradients.[24] As alternatives to miniaturized pumping systems that rely on magnetic fields, there are efforts in developing miniaturized magnet-less vacuum ion pumps. Fomani *et al.* proposed a high vacuum pump that was intended to increase the ion production by producing very large electron currents from field emitter arrays.[28] Another effort utilized a set of electrodes that were biased at certain DC voltages to modestly lengthen the electron trajectories inside the pumping volume, which is similar in concept to the Orbitron pump.[29] Both efforts depend on high density electron streams, which can cause the pressure to rise due to electron-induced gas desorption. This paper describes a miniature, magnet-less RF electron trap that requires substantially fewer electrons. This trap uses only RF electric fields to confine electrons and lengthen their integrated trajectories to enhance ionization efficiency at high vacuum levels, as schematically shown in Fig. 1(b). The trap is intended to be incorporated into a miniaturized ion pump—replacing the Penning cell and permanent magnets—to realize magnet-less ionization and pumping of gases at low pressures, enabling active pressure control of atomic microsystems.

This paper presents modeling results of RF electron trapping in ultrahigh vacuum conditions, while experimental studies are presented in an accompanying paper.[30] The operation of the RF electron trap is first described by an analytical model presented in Sec. II and the Appendix. The computational model used in this study is also described in Sec. II. The results from the computational study are discussed in Sec. III, including the implications for ion pump performance utilizing this trapping approach. Conclusions are given in Sec. IV.

II. DESCRIPTION OF THE TRAPPING CONCEPT AND MODEL

The RF electron trap concept is shown in Fig. 1(b). Electrons can be generated by a commercially available electron gun system or an integrated field emitter array. The relatively low energy electrons drift through the first grid

electrode and become subsequently trapped between the first and second grid electrodes by the application of an RF voltage across the electrodes. The electrons oscillate in this intraelectrode region, and the extended trajectory and added kinetic energy become sufficient to ionize the target gas. Ions build up in the intraelectrode region while the RF voltage is applied, as the high frequency RF electric fields do not tend to appreciably accelerate the relatively massive ions. After a sufficient ionization time, the RF voltage is switched off, and a DC voltage is applied to the grid cathode, causing the ions to accelerate toward it. The sequence is then repeated. In this way, the RF electron trap enables a magnetless ion pump.

A. Analytical model

A one-dimensional analytical model for demonstrating the RF electron trapping concept is schematically shown in Fig. 2. Two parallel electrodes, denoted RFA and RFB, are separated by a gap, d. In order to trap and oscillate the electrons between the RFA and RFB electrodes, an RF voltage $|V_{RF}|$ is applied at RFA at a frequency f_{RF}, while RFB is grounded to limit the electron excursion within $d/2$, half of the gap between the parallel electrodes. Based on the Lorentz force on an electron,[31] for a given f_{RF} and d, the RF electron trapping will only occur if

$$|V_{RF}| \leq \frac{2m_e(\pi f_{RF})^2}{q}(d)^2, \tag{1}$$

where m_e is the mass of an electron and q is the fundamental charge of an electron. This expression is derived in the Appendix. The equal sign in Eq. (1) denotes the optimum RF trapping voltage $|V_{RF}^*|$. The optimum value enables the electrons to traverse the entire electrode gap during an RF cycle. For values of $|V_{RF}|$ larger than $|V_{RF}^*|$, electrons are accelerated into the electrodes before being turned back, and no RF trapping occurs. For $|V_{RF}|$ smaller than $|V_{RF}^*|$, trapping still occurs; however, the electrons oscillate within a length shorter than the interelectrode gap. The confinement of the electrons between the two RF electrodes is greater. Therefore, an electron trapping confinement factor

k_{trap} is defined based on Eq. (1) to describe a one-dimensional established RF electron trap

$$k_{trap} = \sqrt{\frac{2m_e}{|V_{RF}|q}}\pi f_{RF}d. \tag{2}$$

For a chosen $|V_{RF}|$, f_{RF}, and d, no RF electron trapping occurs when the confinement factor $k_{trap} < 1$. Trapping occurs for $k_{trap} = 1$, and the excursion of the electron equals the entirety of the electrode gap. As k_{trap} exceeds 1, the electron confinement is increased, with the electron excursion reduced within the electrode gap. For example, for a d value of 5 mm and a f_{RF} value of 240 MHz, the optimum RF trapping voltage amplitude $|V_{RF}^*|$ is 200 V, resulting in all electrons in the trap limited to an excursion amplitude of exactly $d/2$ and a k_{trap} value of 1. A k_{trap} value of greater than 1, for example as a result of a lower $|V_{RF}|$, would result in more tightly confined electrons between the RFA and RFB electrodes. Alternatively, the k_{trap} value can be used as an indicator of the stability of the electron trajectories in the face of positional or velocity perturbations. A k_{trap} value of greater than 1 allows electrons that are initially "out of phase" with the RF voltage from a positional or energy standpoint to still remain within the electrode gap while cycling. Although this can be a possible advantage, operating under conditions with a very high k_{trap} value will generally result in reduced time-averaged electron energy for a given RF power level.

B. Computational model

The hybrid plasma equipment model (HPEM) modeling framework was used to simulate the scaling of electron trapping. The HPEM is a two-dimensional fluid-hybrid plasma simulation platform which consists of separate modules—each of which addresses different physical phenomena—and exchanges information between the modules in a hierarchical manner.[32] The modules are executed sequentially on time scales short enough to resolve the pulse durations of the applied voltages. A single execution cycle through all modules used in a simulation, with each module accepting data from the previous module and providing data for the next in a sequential manner, is called an iteration. The modules are cycled through until a convergence is reached or a specified number of iterations have occurred. In this study, the modules of HPEM utilized are the fluid kinetics-Poisson module (FKPM) and the electron Monte Carlo simulation (eMCS).

The densities of all charged and neutral species and the electric potential are calculated in the FKPM. For all species in the system (electrons, ions, and neutrals), continuity, energy, and momentum equations are integrated in time. The electric potential is obtained from the solution of Poisson's equation using an incomplete lower-upper BiConjugate Gradient sparse matrix solver.[32] Charge densities on surfaces are computed as being due to the fluxes of electrons and ions from the bulk plasma and secondary electrons from other locations collected by those surfaces. A finite volume technique was used to discretize all spatial derivatives.[32]
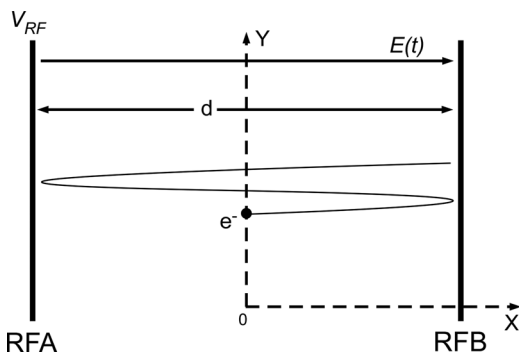

FIG. 2. Schematic of the analytical model of RF electron trapping. V_{RF} is the RF voltage at frequency f_{RF} applied between two electrodes, separated by gap d. $E(t)$ indicates the associated electric field. The electron will travel in an oscillating horizontal trajectory between the plates (the vertical electron motion depicted here is only for clarity).

The basic model as described above is basically a continuum model, whereas the conditions in the trap are at best noncollisional. To address the experimental conditions, described in the companion paper,[30] the model was adapted by modifying the conventional fluid equations to address low pressure. These modifications include using slip boundary conditions, which allow for velocities to be parallel to the surface at the boundary. In the absence of collisions which redirect velocities parallel to a boundary into the surface, velocities parallel to a surface need not decrease when approaching the boundary. A second modification is limiting transport speeds of neutral species to be no greater than the thermal speed. This limitation recognizes that the increase in diffusion coefficients and mobilities at low pressure can produce unphysically large transport speeds due to the mean free paths exceeding cell dimensions. The end result of these modifications is that the gradients in the densities of all species are less severe than at pressures for which continuum transport dominates and in the absence of local sources (such as in the trap itself) would produce nearly uniform densities.

The eMCS is used to derive electron energy distributions (EEDs) for both low energy electrons resulting from ionization processes, referred to as bulk electrons, and for the transport of electrons from the electron beam source, referred to as beam electrons. The algorithms used in the eMCS are discussed in detail in Ref. 32. Briefly, electric fields from the FKPM are recorded as a function of the position and phase during the RF cycle, and RF-cycle-averaged densities of collision partners are transferred to the eMCS. These electric fields are used to advance trajectories of pseudoparticles representing electrons in the eMCS. When computing EEDs for bulk electrons, source functions from the FKPM are used for the production of electrons. These source functions include spatially dependent rates of ionization due to the electron impact and heavy particle processes such as Penning ionization. The source of beam electrons is specified by the current density of the electron emitter and secondary electrons produced by fluxes of ions and excited states, which are obtained from the FKPM. Statistics are collected on the position and energy of electrons on each advance of their trajectories to produce EEDs, which are then used to produce rate coefficients for electron impact events. The end results are separate sets of rate coefficients for electron impact events resulting from the EEDs for bulk and beam electrons. When combined with densities of species from the FKPM, these rate coefficients are used in the continuity equations in the FKPM for sources of species. Electrons in the eMCS that fall below 4 eV are removed from the eMCS for the beam electrons and are used as source functions in the bulk electron continuity equation. The electric field is updated when the FKPM and eMCS are sequentially and iteratively called during the execution of the model.

The model developed in this study is computationally intensive. In order to benefit from multicore computer architectures, algorithms in the HPEM are parallelized using OpenMP directives. Since the HPEM consists of many different modules each having separate algorithms which are executed sequentially for relatively short times, it is difficult to amortize the computational overhead in launching parallel threads. For this particular implementation of the HPEM, the overall improvement factor in execution time with respect to serial execution is 2.6 on eight cores using the Intel Fortran Compiler and 2.8 GHz Intel Xeon processors.

III. PARAMETRIC MODELING RESULTS AND DISCUSSION

A schematic of the geometry used in modeling of the electron trap is shown in Fig. 3. Two gridded electrodes are separated by a stack of ceramic-grounded metal-ceramic spacers forming the walls of the electron trap with dimensions of 0.7 cm tall × 1 cm wide. The ceramic spacer has a thickness of 1 mm and a relative permittivity of 6.8. The top electrode is RF powered, while the bottom electrode is grounded. The grid is 0.5 mm thick and has openings of 1.75 mm. The electrons are injected into the intragrid (trapping) region from an electron beam source (0.8 cm diameter emitting area) located at the bottom of the domain, 1 cm below the grounded electrode. The computational domain, 3.4 cm tall × 1.8 cm wide, is discretized in a Cartesian coordinate system on a grid of 140 × 75 cells with symmetry about the central y-axis.

The first-principles model described in the Appendix is applicable to an idealized geometry, which provides insight into the efficiency of the trap. Nonidealities—such as fringing electric fields near the grid electrodes and from charged dielectric surfaces and the ionization cross-section dependency on electron energy—are not considered in this model and are more appropriately explored with the computational model. Based on the first-principles model and the power budget for the experimental device, a parameter range was generated in which electron trapping is likely to occur with an RF modulated electric field. This parameter range was investigated using the two-dimensional computational model. In the base case, the computational domain is initially filled with 80 nTorr of helium at room temperature.
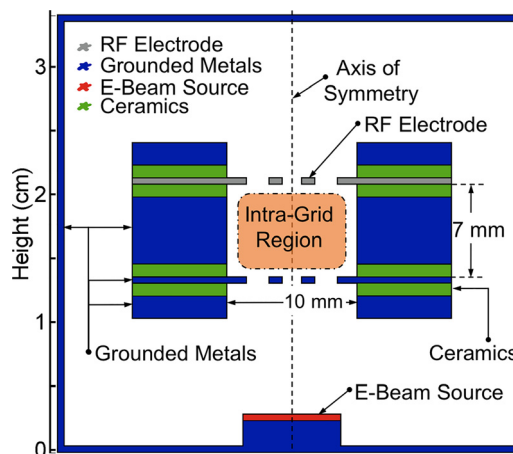

FIG. 3. (Color online) Geometry of the electron trap used in our model and patterned after the experiments described in the companion paper, Ref. 30.

The top electrode is powered by a 150 V amplitude potential oscillating at 150 MHz, which is the operating signal for the experimental device. The electron beam is assumed to provide a uniform electron flux of 40 μA (current density of $\approx$1 μA/mm^2) with an initial electron energy of 15 eV.

The cycle-averaged electron and helium ion densities are shown in Fig. 4 for the base case. Both the densities are concentrated in the intragrid region (trapping region or trap). Electrons injected from the electron beam, having an initial energy of 15 eV, travel to the grounded grid electrode and, depending on the phase of the RF voltage, are repelled or are able to pass through the grid to the trapping region. Those electrons physically striking the grid are collected. Again, depending on the phase of the RF voltage at the time the beam electron passes into the trapping region, the electron may be trapped, may pass through the top grid, or may be accelerated into one of the grids and be collected. Those electrons that are trapped oscillate between the electrodes, during which time they will collide with and ionize helium atoms. At some point, the electrons strike the walls, thereby charging dielectric surfaces or contributing to electrode current.

Based on the analytical model, the electron excursion time (i.e., the number of RF cycles that an electron will survive before hitting a wall or exiting the trap) depends on the electron energy when entering the trap at the grounded electrode and the phase of RF at the instant the electron enters the trap. The longer the excursion time, the higher the probability of an electron colliding with a helium atom. In order for the collision to be an ionization event, the electron energy should be at least as high as the ionization threshold in helium, which is 24.6 eV. The electron density in the trap is increased on a cycle to cycle basis until it reaches the steady state (after 10–20 cycles, with each cycle being a few nanoseconds in period).

The densities of the ionization rate due to the impact of gas molecules with the bulk electrons (S_{bulk}) and due to the impact of gas molecules with the beam electrons (S_{ebeam}) are shown in Fig. 5. The spatial distribution of S_{bulk} mirrors the profile of the electron density and peaks at 6.1 $\times$ 10^6 cm^{-3} s^{-1}. After leaving the surface of the electron beam emitter, the trajectories of electrons are vertical and perpendicular to the surface of the electron beam emitter. With an energy of 15 eV, these electrons cannot ionize helium atoms, which have an ionization potential of 24.6 eV. Ionization thus can only occur by the beam electrons that have been accelerated by the RF field. In principle, no ionization is expected to occur in the region between the electron beam emitter and the bottom grid because the beam electrons are in a nearly field-free region—both the emitter surface and the bottom grid electrode are grounded. However, ionization in this region clearly occurs. The ionization tracts resulting from the beam electrons in this region are caused by electrons being reflected by the RF electric fields inside the trap and passing back through the bottom grid. It is for this reason the ionization tracts are shadowed by the bottom grid. The ionization tracts above the intragrid region result from beam electrons accelerated inside, but then escaping from, the trap. As a result of the fringing electric fields that penetrate through the holes in the grid, off-axis components to the electron velocity are generated and these produce the ionization tracts that are at an angle to the axis. In the full pump configuration, a grounded sorption layer will be integrated above the grid cathode, thus blocking these electrons from escaping and forming the external ions. The value of S_{ebeam} peaks at a location within the trap with a value of 90 $\times$ 10^6 cm^{-3} s^{-1}. The synergistic effect of the electron beam source and the RF modulated field results in the efficient trapping of electrons in the intragrid region.

In the simulations, the base pressure was varied from 40 and 120 nTorr with other parameters remaining the same. The resulting electron density and S_{bulk} on the centerline (radius = 0) are shown in Fig. 6. The electron density is relatively
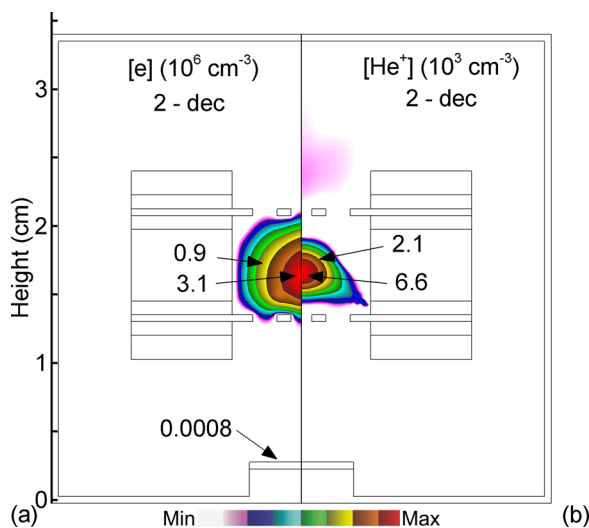
FIG. 4. (Color online) Plasma properties for the base case conditions (He, 80 nTorr, 150 MHz, 150 V, 15 eV, 40 μA). (a) Electron density, and (b) He$^+$ density. Densities are plotted on a 2-decade log scale with the maximum values indicated.
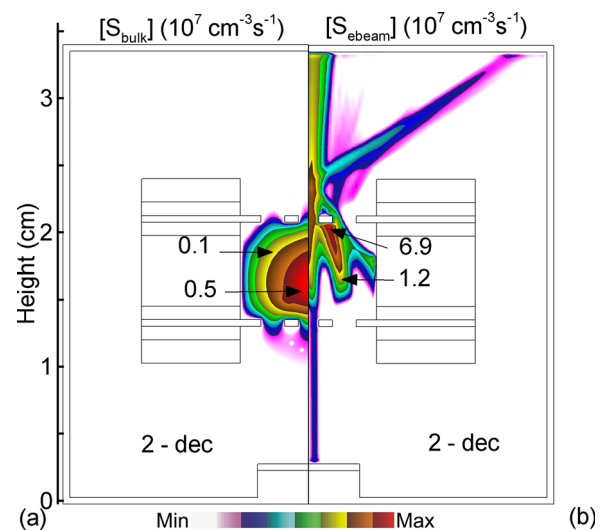
FIG. 5. (Color online) Plasma properties for the base case conditions (He, 80 nTorr, 150 MHz, 150 V, 15 eV, 40 μA). Electron impact ionization rate densities by (a) bulk and (b) beam electrons. Densities are plotted on a 2-decade log scale with the maximum values indicated.
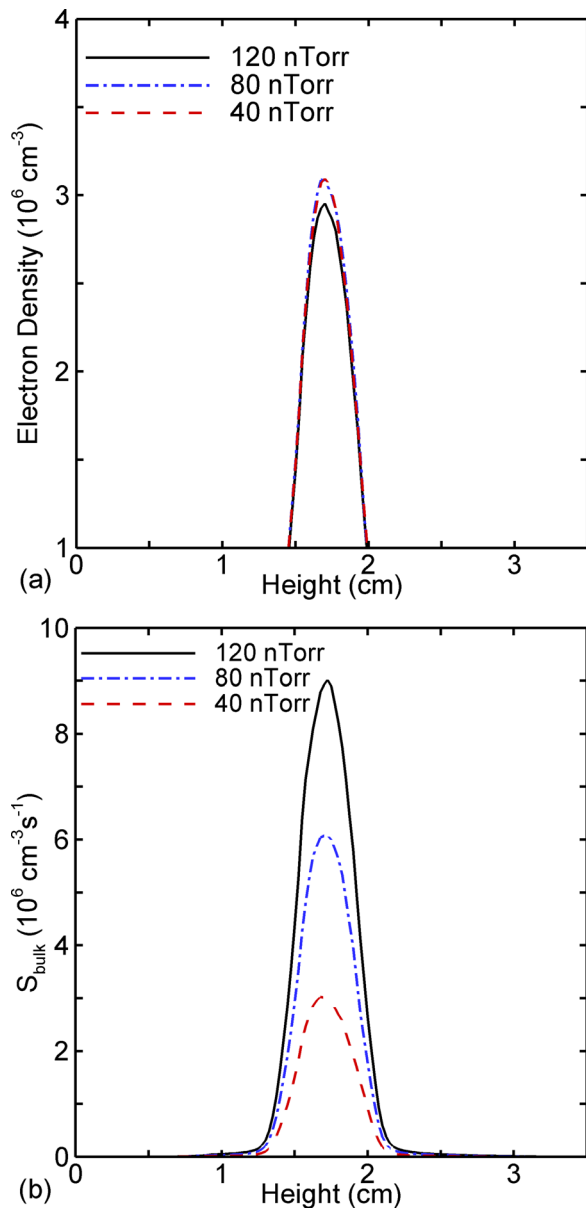
FIG. 6. (Color online) Electron trapping for gas pressures of 40, 80, and 120 nTorr (He, 150 MHz, 150 V, 15 eV, 40 μA). (a) Electron densities and (b) electron impact ionization rate densities by bulk electrons on the center line as a function of height.
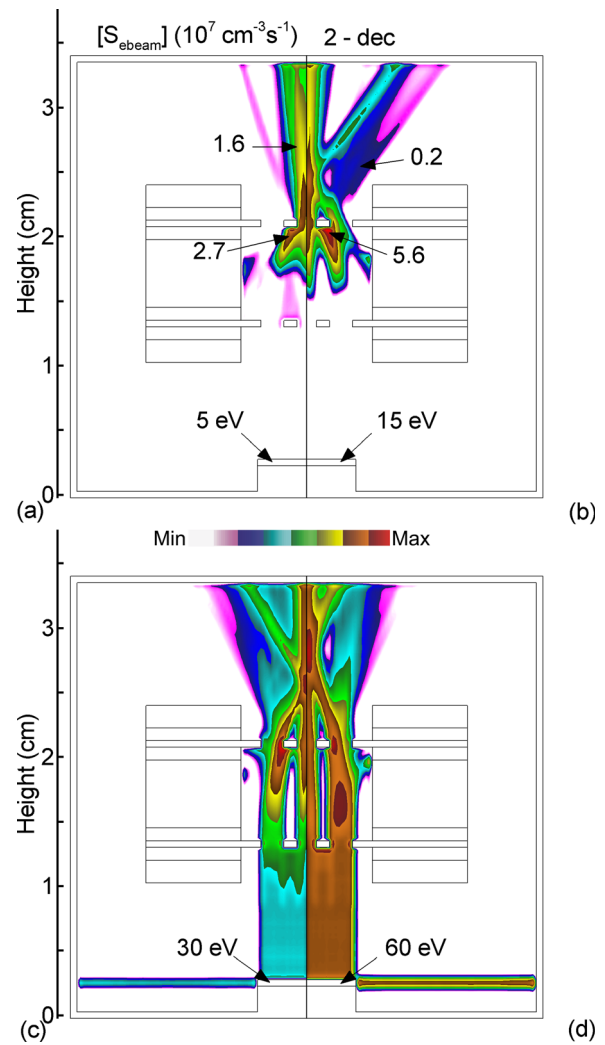

FIG. 7. (Color online) Electron impact ionization rate densities by electron beam electrons for the initial e-beam electron energies of (a) 5 eV, (b) 15 eV, (c) 30 eV, and (d) 60 eV (He, 80 nTorr, 150 MHz, 100 V, 40 μA).

insensitive to the pressure changes from 40 to 120 nTorr. These pressure changes are not sufficient to significantly affect the electron excursion time for a given set of fixed external conditions such as the gap distance, frequency, and voltage. Since the simulated pressure has been linearly increased, the helium density linearly increases, and so, S_{bulk} also increases. However, the ionization rate is determined primarily by the concentration of injected beam electrons, and so, the trapped electron density does not significantly change.

In additional simulations, the initial energy of electrons injected from the electron beam source was varied between 5, 15, 30, and 60 eV, and the resulting ionization rate densities by beam electrons, S_{ebeam}, are shown in Fig. 7 for the RF voltage amplitude of 100 V. For initial energies <24.6 eV,

ionization does not generally occur below the lower grounded grid in the absence of back-reflections from the trap. As the energy of the electron beam increases above 24.6 eV, ionization occurs below the trap and there is higher likelihood that the beam electrons may pass through the trap. At the same time, the ionization rate increases within the trap as well. The horizontal tracts of ionization for initial beam energies of 30 and 60 eV result from electrons that are emitted from the sides of the source.

The density of trapped electrons is sensitive to the electron beam current. The electron density on the centerline (R = 0 cm) for e-beam currents of 20–2000 μA and peak electron density along this line as a function of current are shown in Fig. 8. The peak electron density varies with electron beam current fairly linearly over this range of current, which indicates that the trap is not likely to saturate over the range of conditions studied here.

The peak electron densities in the trap as a function of RF voltage for a fixed frequency of 150 MHz are shown in Fig. 9. The peak electron densities have their maximum value for
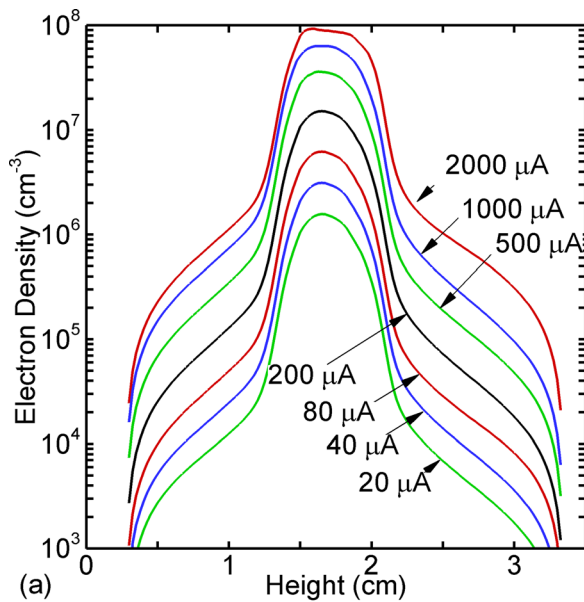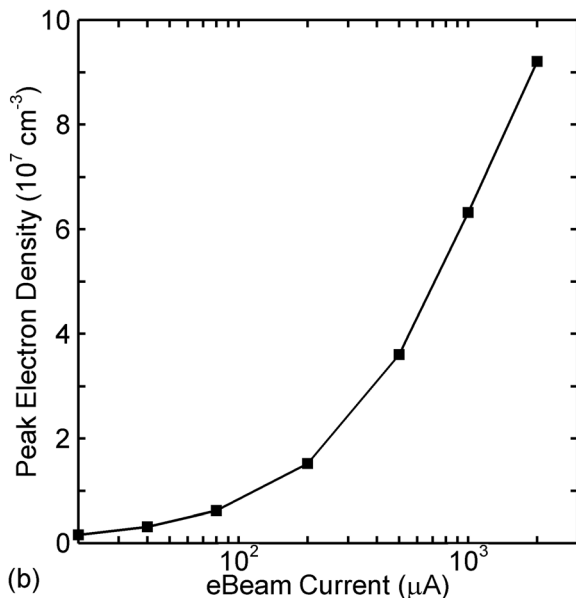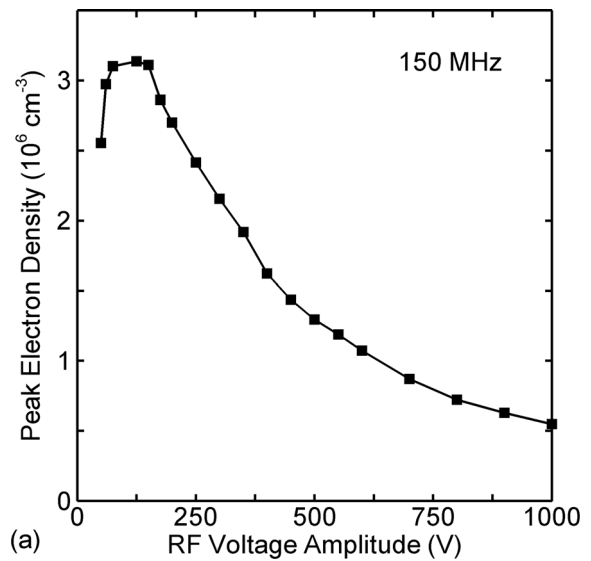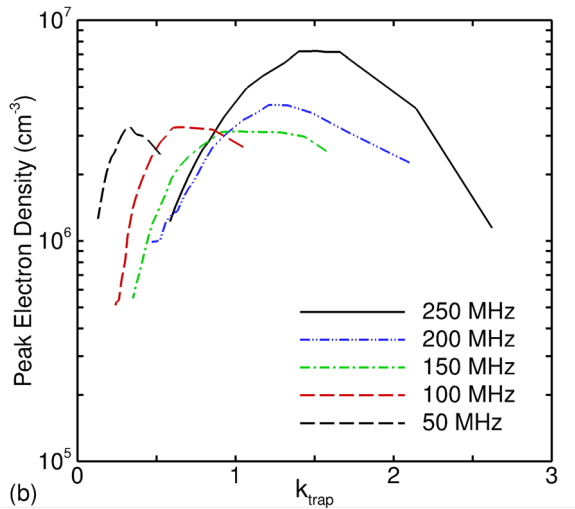
FIG. 8. (Color online) Plasma properties as a function of e-beam current: (a) Electron densities as a function of height on the axis for different electron beam currents. (b) Peak electron density as a function of electron beam current (He, 80 nTorr, 150 MHz, 150 V).

FIG. 9. (Color online) Maximum electron densities for an e-beam initial energy of 15 eV as a function of (a) applied RF voltage at 150 MHz and (b) trap confinement factor k_{trap} for RF frequencies of 50, 100, 150, 200, and 250 MHz (He, 80 nTorr, 40 μA).

RF voltage amplitudes between 100 and 200 V. Higher voltages either reflect the beam electrons or accelerate the beam electrons out the top of the trap. The results in Fig. 9(a), as well as those for frequencies of 50–250 MHz, are recast as a function of k_{trap} in Fig. 9(b). Interpretation of these numerical results is given in Fig. 10, which shows k_{trap} as a function of the RF voltage amplitude for different frequencies for the model geometry as calculated by the analytical model, Eq. (2). As shown in Fig. 9(a), the peak trapped electron density for 150 MHz occurs for values of k_{trap} between 1 and 1.6, which corresponds to voltages of 200 and 100 V, respectively. These values are in a good agreement with the predictions of the analysis discussed in the Appendix. These trends are also in good agreement with experimental observations (presented in our accompanying paper[30]).

For the other values of the frequencies, the trends do not fully obey the predictions from the first-principles analysis. The maximum trapped electron densities occur for voltage amplitudes of 100 to 250 V, corresponding to k_{trap} values between 0.3 and 1.7. The deviation of the analytical theory from the results from the model is likely due to a number of effects not captured in the simplified analysis, including non-uniformities in the electric field that produce losses from the trap even at optimum frequencies, electron repulsion from charged surfaces, and electrons produced by ionization events.

The modeling results can allow some quantification of how this RF electron trap could be used in an ion pump. As shown in Figs. 5 and 7, ionization rates in this trap can reach $\sim 10 \times 10^6$ ions/cm^3/s during the application of RF power. As such, if all ions produced are physisorbed in a sorption layer via the application of pulsed DC (with a required duration of only a millisecond), then a RF duty cycle of only

10% could theoretically result in $0.1\,\mathrm{nTorr/cm^3/s}$ pumping rates. These are only order-of-magnitude calculations but illustrate the potential utility of this trapping scheme. The reduced duty cycle could be used to reduce the required average RF power while still maintaining useful pumping rates.

IV. CONCLUSIONS

The electron trapping concept investigated here uses RF electric fields to lengthen the electron trajectory in the trap, without the use of magnetic fields. Analytical and parametric numerical models were applied to examine the operating conditions of the trap. The analytical model predicts a trap confinement factor, k_{trap}, which indicates the combination of voltage, frequency, and trap size that should result in trapping. The parametric numerical study has shown that the peak electron density within the trap is proportional to the electron beam current (2×10^7 cm^{-3} density for a $40\,\mu\mathrm{A}$ current) and exhibits a peak for a range of RF voltage amplitudes (100–250 V for frequencies from 50 to 250 MHz) that is reasonably well represented by the analytical model. The results from the model presented here on a proof-of-concept geometry demonstrate that electrons can be trapped with this approach. The electron density in the trapping region can be increased by three or more orders of magnitude compared to the electron beam density. These results indicate the potential of this electron trapping approach in miniaturized, magnet-less ion pumps, which would be particularly useful in atomic microsystems. These results are in good qualitative agreement with the experimental results presented in the accompanying paper.[30]

ACKNOWLEDGMENTS

APPENDIX

The rationale of the RF electron trap results from a first-principles analysis of a one-dimensional idealized geometry consisting of two electrodes (grounded and RF powered) separated by a gap of dimension d, as shown in Fig. 2. Electrons in this electric field experience a Lorentz force

$$F = -qE = \frac{q}{d}V_{\mathrm{RF}}\sin(2\pi f_{\mathrm{RF}}t + \phi),\qquad(\mathrm{A1})$$

where q is the fundamental charge, E is the electric field, V_{RF} and f_{RF} are the amplitude and frequency of the RF voltage, and ϕ is the RF phase. The electron path is not affected by the presence of other electrons, ions, or neutrals—which is a fair assumption in the low particle density, low pressure conditions studied here. In an ideal trap, the electron travels the entire gap between the electrodes periodically and

indefinitely. This is considered an "ideally trapped" electron. The position of such an ideally trapped electron at time t is

$$x^*(t) = \frac{d}{2} - \frac{d}{2}\sin(2\pi f_{\mathrm{RF}}t + \phi),\qquad(\mathrm{A2})$$

where superscript "$*$" denotes the ideal condition. Combining the Lorentz force and Newton's Law and comparing with Eq. (A2), one can derive that the ideal RF voltage V_{RF}^*, the ideal initial position x_0^*, and ideal initial velocity v_0^* of the ideally trapped electron are

$$V_{\mathrm{RF}}^* = \frac{2m_e(\pi f_{\mathrm{RF}})^2}{q}(d)^2,\qquad(\mathrm{A3})$$

$$x_0^* = \frac{d}{2} - \frac{d}{2}\sin(\phi),\qquad(\mathrm{A4})$$

$$v_0^* = -f_{\mathrm{RF}}\pi d\cos(\phi),\qquad(\mathrm{A5})$$

where m_e is the electron mass. Equations (A3)–(A5) show that once an RF frequency and gap have been chosen, then the optimum voltage is determined. The choice of frequency (and initial RF phase) will determine which "slice" of the trap (x_0 position) will be ideally trapped *if* the electrons at that slice have the ideal initial velocity v_0^*. In other words, only the slice of electrons with the initial position x_0^* and initial velocity v_0^* will be ideally trapped.

A compromise can be made to decrease the path length for electrons in the trap but allow the electron excursion to be periodical and indefinite (provided that appropriate initial conditions are present). This can be achieved by increasing the frequency by a confinement factor of $k_{\mathrm{trap}} \geq 1$,

$$V_i = \frac{2m_e}{q}\left(\frac{\pi f_{\mathrm{RF}}}{k_{\mathrm{trap}}}\right)^2(d)^2,\qquad(\mathrm{A6})$$
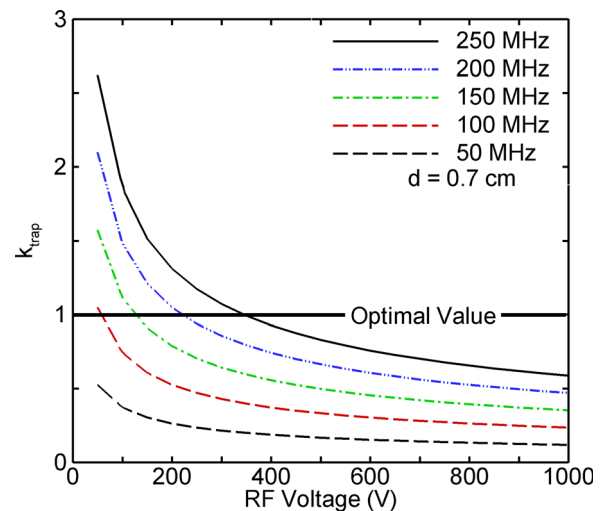

FIG. 10. (Color online) Trap confinement factor k_{trap} as given by the analytical theory as a function of RF voltage for fixed frequencies of 50, 100, 150, 200, and 250 MHz.

where subscript "*i*" denotes the "nonoptimum" condition. Using Eq. (A6) along with the Lorentz force and Newton's law, it can be found that the electrons will oscillate around the center of the trap with the position described as

$$x(t) = \frac{d}{2} - \frac{d}{2k_{\text{trap}}^2} \sin\left(2\pi f_{\text{RF}} k_{\text{trap}} t + \phi\right), \qquad (A7)$$

when the initial conditions are

$$x_{0,i} = \frac{d}{2} - \frac{d}{2k_{\text{trap}}^2} \sin(\phi), \qquad (A8)$$

$$v_{0,i} = -f_{\text{RF}} \pi d \frac{\cos(\phi)}{k_{\text{trap}}}. \qquad (A9)$$

The benefit of the reduced excursion described using Eq. (A7) is that a "band" of electrons with initial velocity $v_{0,i}$ and initial position $x_0 = x_{0,i} + d/2\Delta x$ also remains within the trap. In this case, the electron position will be

$$x(t) = \frac{d}{2}(1 + \Delta x) - \frac{d}{2k_{\text{trap}}^2} \sin(2\pi f_{\text{RF}} t + \phi). \qquad (A10)$$

To remain in the trap, one should ensure that $0 \leq x(t) \leq d$ for all values of *t*. Thus, the electrons with

$$\frac{1}{k_{\text{trap}}^2} - 1 \leq \Delta x \leq 1 - \frac{1}{k_{\text{trap}}^2}, \qquad (A11)$$

will remain in the trap for all time. As an example, if $k_{\text{trap}} = 1.1$, then a band with $-0.18 \leq \Delta x \leq 0.18$ will be trapped (i.e., up to 18% of *d*). The value of k_{trap} as a function of RF voltage for various fixed values of frequencies and a fixed gap size of $d = 0.7$ cm is shown in Fig. 10.

[1] J. Zook, D. Burns, H. Guckel, J. Sniegowski, R. Engelstad, and Z. Feng, Sens. Actuators, A **35**, 51 (1992).
[2] C. Borde, Metrologia **39**, 435 (2002).
[3] S. Knappe, "MEMS atomic clocks," in *Comprehensive Microsystems*, edited by Y. B. Gianchandani, O. Tabata, and H. Zappe (Elsevier, Oxford, 2008), Chap. 3.18, pp. 571–612.
[4] S. Knappe, P. Schwindt, V. Gerginov, V. Shah, L. Liew, J. Morelan, H. Robinson, L. Hollberg, and J. Kitching, J. Opt. A: Pure Appl. Opt. **8**, S318 (2006).
[5] R. Lutwak *et al.*, *36th Annual Precise Time and Time Interval (PTTI) Meeting* (2004), pp. 339–354.
[6] Y. Y. Jau, H. Partner, P. D. D. Schwindt, J. D. Prestage, J. R. Kellogg, and N. Yu, Appl. Phys. Lett. **101**, 253518 (2012).
[7] D. R. Scherer *et al.*, *46th Annual Precise Time and Time Interval Systems and Application Meeting* (2014), pp. 154–163.
[8] K. Nelson, K. Salit, J. Kriz, D. Sandquist, and J. Sebby-Strabley, *2012 IEEE/ION Position Location and Navigation Symposium (PLANS)* (2012), pp. 1094–1098.
[9] T. Müller, M. Gilowski, M. Zaiser, P. Berg, C. Schubert, T. Wendrich, and E. M. Rasel, Eur. Phys. J. D **53**, 273 (2009).
[10] B. Canuel, F. Leduc, D. Holleville, A. Gauguet, A. Virdis, A. Clairon, and P. Bouyer, Phys. Rev. Lett. **97**, 010402 (2006).
[11] G. Wu, D. Xu, B. Xiong, Y. Wang, and Y. Ma, J. Microelectromech. Syst. **21**, 1484 (2012).
[12] L. Mauri, E. Rizzi, M. Moraja, and M. Campaniello, *2013 Microelectronics Packaging Conference (EMPC)* (2013), pp. 1–4.
[13] D. Sparks, N. Najafi, and B. Newman, U.S. patent 7,789,949 (7 September 2010).
[14] D. Sparks, N. Najafi, and S. Massoud-Ansari, IEEE Trans. Adv. Packag. **26**, 277 (2003).
[15] A. Dellis, V. Shah, E. Donley, S. Knappe, and J. Kitching, Opt. Lett. **41**, 2775 (2016).
[16] G. L. Saksaganskii, *Getter and Getter-Ion Vacuum Pumps* (Harwood Academic, Amsterdam, 1994).
[17] B. Kim *et al.*, J. Appl. Phys. **105**, 013514 (2009).
[18] D. R. Scherer, D. B. Fenner, and J. M. Hensley, J. Vac. Sci. Technol., A **30**, 061602 (2012).
[19] A. Besharatian, K. Kumar, R. L. Peterson, L. P. Bernal, and K. Najafi, *IEEE International Conference on Microelectromechanical Systems (MEMS)*, Paris, France (2012), pp. 1001–1004.
[20] H. Zhou, H. Q. Li, V. Sharma, and M. A. Schmidt, *IEEE International Conference on Microelectromechanical Systems (MEMS)*, Cancun, Mexico (2011), pp. 1095–1098.
[21] S. An, N. K. Gupta, and Y. B. Gianchandani, J. Microelectromech. Syst. **23**, 406 (2014).
[22] M. Audi and M. de Simon, Vacuum **37**, 629 (1987).
[23] K. M. Welch, *Capture Pumping Technology*, 2nd ed. (Elsevier, Amsterdam, 2001).
[24] S. R. Green, R. Malhotra, and Y. B. Gianchandani, J. Microelectromech. Syst. **22**, 309 (2013).
[25] T. Grzebyk, A. Górecka-Drzazga, and J. A. Dziuban, Sens. Actuators, A **208**, 113 (2014).
[26] P. D. D. Schwindt, Y. Y. Jau, H. Partner, A. Casias, A. R. Wagner, M. Moorman, R. P. Manginell, J. R. Kellogg, and J. D. Prestage, Rev. Sci. Instrum. **87**, 053112 (2016).
[27] J. Kitching, S. Knappe, and E. Donley, IEEE Sens. J. **11**, 1749 (2011).
[28] A. A. Fomani, L. F. Velásquez-García, and A. I. Akinwande, *Technical Digest of 27th International Vacuum Nanoelectronics Conference (IVNC)* (2014), pp. 210–211.
[29] A. Basu and L. F. Velásquez-García, J. Micromech. Microeng. **26**, 124003 (2016).
[30] S. Deng, S. R. Green, A. H. Markosyan, M. J. Kushner, and Y. B. Gianchandani, "Miniaturized magnet-less RF electron trap. II. Experimental verification," J. Vac. Sci. Technol., B **35**, 042002 (2017).
[31] O. D. Jefimenko, *Electricity and Magnetism: An Introduction to the Theory of Electric and Magnetic Fields*, 2nd ed. (Electret Scientific, Waynesburg, PA, 1989).
[32] M. J. Kushner, J. Phys. D **42**, 194013 (2009).